JMSR 1(2) (2025)

Journal of Material Science and Radiation

https://journals.balaipublikasi.id/jmsr

Influence of CuO Addition on the Structural, Magnetic and Electrical Properties of $Nd_{0.67}Sr_{0.33}MnO_3$ Composites

L.N. Lau[1,2], X.T. Hon[1], K.P. Lim[1]*, N.A. Mazlan[1], M.M. Awang Kechik[1], S.K. Chen[1], M.K. Shabdin[1], and A.H. Shaari[1]

[1] Superconductor and Thin Film Laboratory, Department of Physics, Faculty of Science, Universiti Putra Malaysia, 43400 UPM Serdang, Selangor Darul Ehsan, Malaysia.
[2] International College of Semiconductor Technology, National Yang Ming Chiao Tung University, Hsinchu 30010, Taiwan.

Received: May 8, 2025
Revised: July 12, 2025
Accepted: August 25, 2025
Published: August 31, 2025

Corresponding Author:
K.P. Lim
limkp@upm.edu.my

Abstract: Colossal magnetoresistance (CMR) materials are widely studied to be applied in magnetic sensing elements. The incorporation of a secondary oxide phase into manganites has been explored to improve low-field magnetoresistance (LFMR). In this study, polycrystalline $Nd_{0.67}Sr_{0.33}MnO_3$ (NSMO) was synthesised via the sol-gel method, and different contents of CuO nanopowder were added to form (1–x) NSMO: x CuO composites. The structural, magnetic, and electrical properties of the composites were characterised by X-ray diffraction (XRD), AC susceptibility (ACS), and Hall effect measurement (HMS). XRD results confirmed the orthorhombic structure in all samples and indicated no reaction between NSMO and CuO, suggesting that CuO segregates at the grain boundaries or surfaces of NSMO grains. Magnetic measurements revealed negligible variation in the Curie temperature (T_C), while electrical measurements showed a suppression of the metal–insulator transition temperature (T_{MI}). Although LFMR was more pronounced at lower temperatures, no enhancement was observed in the NSMO composites compared to its parent compound. This behaviour is attributed to spin-polarised tunnelling, which dominates LFMR and is primarily dominated by the nanoscale NSMO achieved through sol-gel synthesis. These findings offer valuable insights into the magnetotransport properties of NSMO:CuO composites and the role of secondary oxide phases in tailoring LFMR.

Keywords: Electrical; CMR, LFMR; Magnetic; Nanopowder; NSMO

Introduction

The hole-doped manganites with a general formula of $RE_{1-x}A_xMnO_3$, where RE is a rare earth ion (RE = La, Nd, Pr) and A is a divalent alkaline earth metal ion (B = Ba, Sr, Ca) have been attracted considerable research interest due to their remarkable colossal magnetoresistance (CMR) properties. Magnetoresistance refers to the change in electrical resistance of a material when subjected to an external magnetic field. The discovery of CMR in manganites has positioned them as promising candidates for spintronic applications, including magnetic memory devices and magnetic field sensors (Xia et al., 2020).

Perovskite manganites exhibit pronounced CMR near the metal-insulator transition and the ferromagnetic–paramagnetic transition (Ng et al., 2018). Their electrical conduction and magnetic behaviour are well explained by the double exchange (DE) mechanism, which involves electron hopping between Mn^{3+} and Mn^{4+} ions (Zener, 2018). There are two types of CMR effects in manganites, namely intrinsic and extrinsic magnetoresistance (Tang et al., 2008). Intrinsic magnetoresistance typically manifests at high magnetic fields (≥ 10 kOe), whereas extrinsic magnetoresistance is more significant at low magnetic fields (Nagaev, 2001). For practical spintronic applications, materials that exhibit strong magnetoresistance under low magnetic fields are highly desirable (Sadhu & Bhattacharyya,

How to Cite:
Lau, L. N., Hon, X., Lim, K. P., Mazlan, N. A., Kechik, M. M. A., Chen, S. K., … Shaari, A. H. (2025). Influence of CuO Addition on the Structural, Magnetic and Electrical Properties of Nd0.67Sr0.33MnO3 Composites. *Journal of Material Science and Radiation*, *1*(2), 49–54. Retrieved from https://journals.balaipublikasi.id/index.php/jmsr/article/view/375

2014). The extrinsic magnetoresistance is attributed to the spin-polarised tunnelling, and it can be achieved by the natural or artificial grain boundaries in manganites (Hwang et al., 1996; Phong et al., 2009). Recently, incorporation of the secondary oxide phase into the manganite system has been widely adopted to enhance low field magnetoresistance (LFMR), as demonstrated by LSMO: NiO (Eshraghi et al., 2007), LSMO: SFO (Zi et al., 2012), LCMO: Sm_2O_3 (Li et al., 2019), LCMO: Al_2O_3 (Thanh et al., 2011), and LSMO: ZnO (Navin & Kurchania, 2018).

In this work, we prepared $Nd_{0.67}Sr_{0.33}MnO_3$ (NSMO) composites by the sol-gel method. The effect of CuO nanopowder addition on the structural, magnetic, and electrical properties were systematically examined. This study aims to provide deeper insights into the magnetotransport properties of (1-x) NSMO: x CuO composites and to explore the potential of secondary oxide phases in enhancing LFMR.

Method

The samples were prepared in 2-stage: the synthesis of NSMO compound via the sol-gel route and the addition of CuO nanopowder. The preparation of NSMO followed the procedures discussed in our previous work (Lau, Lim, Ishak, et al., 2021). NSMO compound that pre-sintered (known as sintering process in that work) at 800 °C was added with different contents of CuO (MTI Corp, 99.99%) nanopowder (30 nm) to form (1-x) NSMO: x CuO composites, where x = 0.00, 0.01, 0.03, 0.05, 0.10, and 0.15. These mixed powders were ground, pressed into pellets, and then sintered at 500 °C for two hours.

The structural characterisation was carried out by an X-ray diffractometer (XRD, Malvern Panalytical X'Pert Pro PW 3040), and Rietveld analysis was performed by HighScore Plus 3.0.5 software. Alternating current (AC) susceptibility was measured by an AC susceptometer (ACS, CryoBIND T) in a magnetic field of 5 Oe at 219 Hz to determine the Curie temperature (T_C). The temperature dependence of the resistivity and magnetotransport were assessed by standard four-point probe method using a Hall effect measurement system (HMS, Lakeshore 7604 HMS) from 80 K to 300 K.

Result and Discussion

Figure 1 shows that all samples are fully crystalline and exhibit $Nd_{0.67}Sr_{0.33}MnO_3$/NSMO as the primary phase. The peaks corresponding to the second phase in composite samples have been matched with CuO, and it is observed that the peak intensity gradually increases with the content. All peaks from XRD patterns can be indexed with NSMO and CuO phases, which implies that no impurities or additional phases were formed in the samples. Rietveld refinement has been performed, and the experimental data were all well-fitted, as demonstrated by the low residual value of R_{WP} and χ^2 in Table 1. The average crystallite size, D, was calculated by Scherrer's equation (Biswas & Keshri, 2025) and listed in Table 1.

$$D = \frac{0.89\,\lambda}{\beta \cos\theta} \quad (1)$$

where $\beta = \beta_{\text{sample}} - \beta_{\text{instrumental}}$, β is the line broadening at half of the maximum intensity (FWHM), λ is the X-ray wavelength (1.5406 Å), and θ is the position of the most intense diffraction peak. There is no growth in crystallite as the CuO increases. Besides that, the lattice parameters obtained from the refinement are almost the same throughout the series, as well as the bond angle and distance. Hence, we can deduce that CuO nanopowder is segregated at the grain boundaries or the surface of NSMO grains (Li et al., 2019).

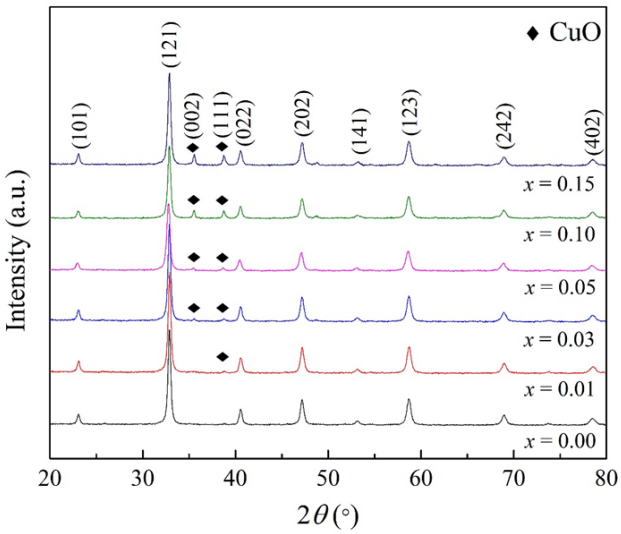

Figure 1. XRD patterns of (1-x) NSMO: x CuO, where x = 0.00, 0.01, 0.03, 0.05, 0.10, and 0.15

Magnetic characterisation reveals that all samples display a ferromagnetic (FM) – paramagnetic (PM) transition, as shown in Figure 2(a). The FM-PM transition is demonstrated by a sharp decline in susceptibility, approaching near-zero values. In Figure 2(b), the Curie temperature (T_C) values are identified from the inflexion point of $d\chi'/dT$ versus T plot, falling within the range of 261 K to 265 K. These results indicate that the addition of CuO does not influence the T_C of NSMO composites, and the individual magnetic phases are preserved. This suggests the absence of interfacial reactions between the two phases, with CuO likely segregated on the surface or outside the NSMO grains, which is an interpretation supported by the XRD results.

Table 1. Rietveld refinement data of NSMO: CuO composites

Compound						$Nd_{0.67}Sr_{0.33}MnO_3$
Reference code						98-010-8658
Structure type						Orthorhombic
Space group						Pnma (62)
CuO content, x	0.00	0.01	0.03	0.05	0.10	0.15
a (Å)	5.443	5.441	5.444	5.437	5.442	5.445
b (Å)	7.685	7.684	7.687	7.681	7.687	7.688
c (Å)	5.463	5.463	5.460	5.465	5.463	5.460
Volume ($Å^3$)	228.526	228.405	228.476	228.227	228.534	228.546
O1-Mn1 (Å)	1.909	1.908	1.908	1.908	1.908	1.908
O1-Mn1 (Å)	2.025	2.025	2.025	2.024	2.025	2.025
O2-Mn1 (Å)	1.933	1.932	1.933	1.932	1.933	1.933
Mn1-O1-Mn1 (°)	157.2	157.2	157.2	157.2	157.2	157.2
Mn1-O2-Mn1 (°)	167.5	167.5	167.6	167.5	167.6	167.6
R_{EXP} (%)	3.584	3.521	3.530	3.780	3.594	3.309
R_P (%)	2.908	3.008	2.932	3.058	2.990	2.770
R_{WP} (%)	3.724	3.831	3.676	3.875	3.835	3.484
Goodness of fit, χ^2	1.080	1.184	1.084	1.051	1.139	1.108
Crystallite size, D (nm)	30.1	28.8	29.8	24.4	28.4	28.4
Compound						CuO
Reference code						98-005-9312
Structure type						Monoclinic
Space group						C12/c1 (15)
a (Å)	-	4.682	4.682	4.682	4.684	4.683
b (Å)	-	3.420	3.420	3.420	3.425	3.425
c (Å)	-	5.125	5.125	5.125	5.131	5.128
Volume ($Å^3$)	-	80.883	80.883	80.883	81.173	81.121

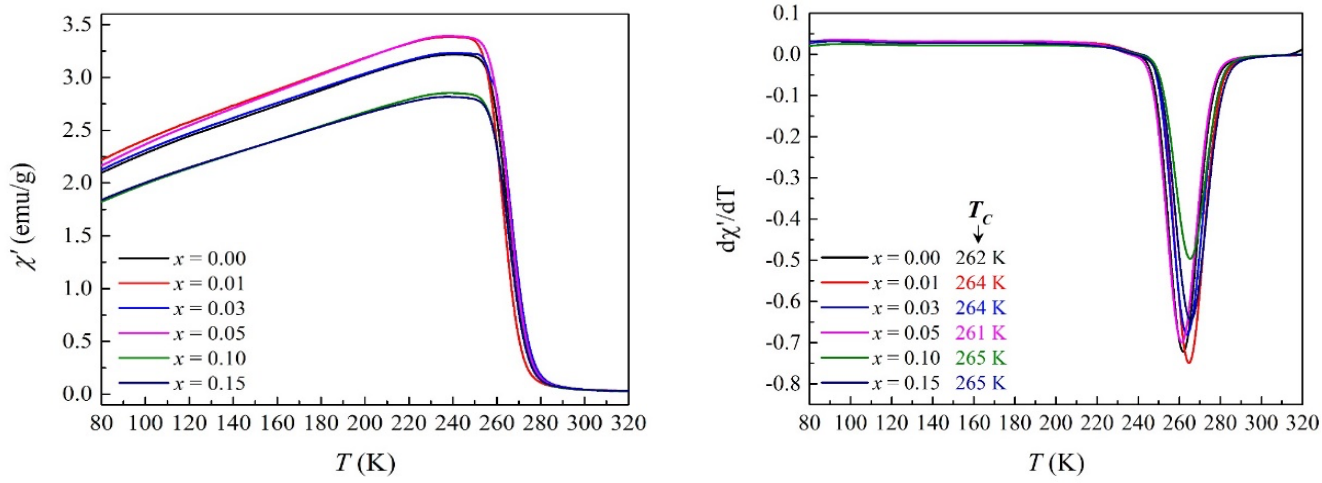

(a) (b)

Figure 2. (a) Temperature dependence of AC susceptibility and (b) $d\chi'/dT$ versus T plot to determine T_C for NSMO: CuO composites

Figure 3 presents the ρ-T plots obtained from electrical measurements. All samples show a distinct metal-insulator transition, characterised by an increase in resistivity with decreasing temperature, reaching a maximum at the transition temperature (T_{MI}), followed by a transition to metallic behaviour. The T_{MI} values of NSMO composites decrease from 162 K to 148 K with increasing CuO content. This shift can be attributed to the presence of a secondary oxide phase (CuO) near the NSMO grains, which likely acts as a barrier to charge carriers and weakens the DE effect (Staruch et al., 2025). This behaviour is consistent with the results obtained from XRD and ACS analyses.

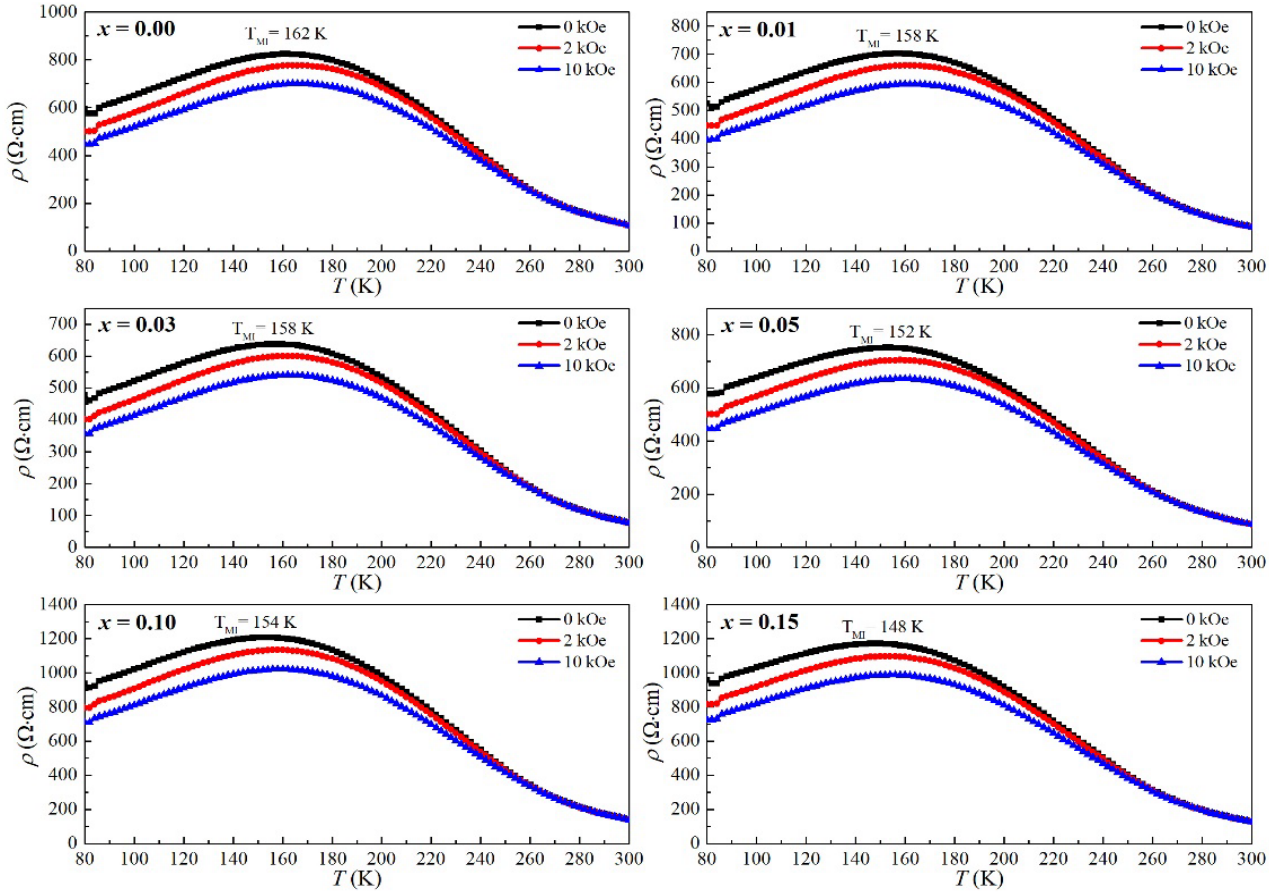

Figure 3. ρ-T plots of (1-x) NSMO: x CuO, x = 0.00, 0.01, 0.03, 0.05, 0.10, and 0.15 from 80 K to 300 K at different magnetic fields

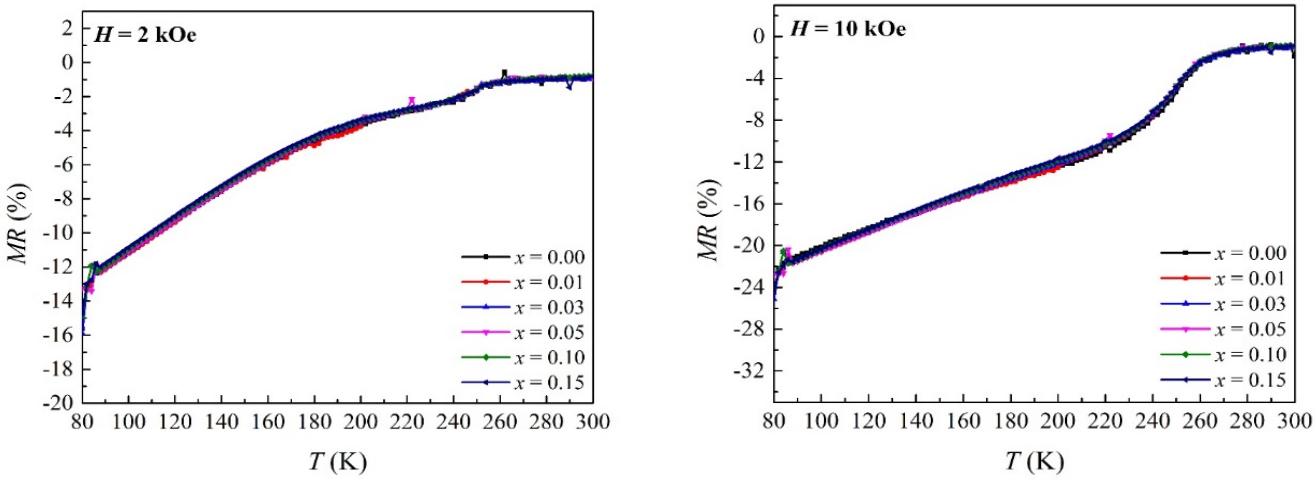

Figure 4. Temperature dependence of *MR*% for NSMO: CuO samples at (a) 2 kOe and (b) 10 kOe

Figure 4 illustrates the temperature dependence of magnetoresistance (*MR*%) for NSMO composites at 2 kOe and 10 kOe. The *MR*% can be calculated using the equation (Hon et al., 2024).

$$MR\ (\%) = \frac{\rho_H - \rho_O}{\rho_O} \times 100 \quad (2)$$

where ρ_O and ρ_H are the resistivities without and with an applied magnetic field, respectively. Figure 4(a) depicts the *MR*% plots at magnetic field of 2 kOe, commonly referred to as low field magnetoresistance (LFMR). It is evident that *MR*% is more pronounced at low temperatures by showing a higher value as the

temperature decreases. This effect is attributed to the spin-polarised tunnelling across grain boundaries, where the disordered spins near the grain boundaries become aligned under an applied magnetic field, enhancing electron hopping and causing a sharp decrease in resistivity in the low-field region (Modi et al., 2017; Zhou et al., 2017). The intrinsic *MR*% plot (10 kOe) is illustrated in Figure 4(b), and it can be explained by the suppression from spin fluctuations, where spins align parallel to the applied magnetic field, resulting in a higher *MR*% value near the T_{MI} or T_C. A noticeable drop in *MR*% occurs at approximately 260 K as the temperature decreases, corresponding to T_C. This drop is more prominent in Figure 4(b), indicating the contribution of intrinsic mechanisms to the magnetoresistance at higher magnetic field (10 kOe). As shown in Figure 4(a), the *MR*% of pure NSMO and its composites increases monotonically with decreasing temperature. However, no enhancement in LFMR is observed in the composites compared to the pure NSMO sample. This observation is consistent with our previously reported findings (Lau et al., 2020; Lau, Lim, Chok, et al., 2021). It can be inferred that the LFMR in this study is primarily attributed to the nanoscale nature of the NSMO, as the material was synthesised via the sol-gel method. Therefore, the addition of CuO does not contribute to any improvement in LFMR performance in the NSMO:CuO composites relative to the pure NSMO sample.

Conclusion

The influence of CuO nanopowder addition on the structural, magnetic, and electrical properties of sol-gel grown $Nd_{0.67}Sr_{0.33}MnO_3$ composites has been successfully investigated. XRD analysis confirmed the absence of reaction between the two phases, with CuO predominantly segregating at the grain boundaries or on the surface of NSMO grains. This is supported by the minimal differences observed in structural parameters and crystallite growth. T_C determined from AC susceptibility measurements, were found to be approximately 260 K, indicating that the individual magnetic phases within the composites are preserved. Electrical characterisation revealed a suppression of the T_{MI} in the composites, which can be attributed to the insulating nature of CuO at the grain boundaries, leading to reduced intergrain connectivity. LFMR was found to be more pronounced at lower temperatures, with higher *MR*% values observed as temperature decreased. However, the composites did not exhibit any improvement in LFMR compared to pure NSMO. This can be explained by the spin-polarised tunnelling mechanism, which governs LFMR is primarily influenced by the nanoscale NSMO particles prepared via the sol-gel method. As a result, the findings of this study provide valuable insights into the magnetotransport properties of NSMO-based composites synthesised using the sol-gel technique..

Acknowledgments
L.N. Lau is grateful for the facilities provided by Universiti Putra Malaysia and National Yang Ming Chiao Tung University.

Author Contributions
Conceptualization, L. N. L and K. P. L; methodology, X. T. H; validation, M. M. A. K and N. A. M; writing—original draft preparation S. K. C.; writing—review and editing, L. N. L., S. K. C., M. K. S., and A. H. S.

Funding
This research was fully funded and supported by Universiti Putra Malaysia (UPM) research grant (GP/2023/9753000).

Conflicts of Interest
The authors declare no conflict of interest.

References

Biswas, S., & Keshri, S. (2025). Enhancement of magnetization with sintering temperature for the perovskite manganite La0.67Sr0.33MnO3. *Physica B: Condensed Matter*, *700*, 416927. https://doi.org/10.1016/j.physb.2025.416927

Eshraghi, M., Salamati, H., & Kameli, P. (2007). The effect of NiO doping on the structure, magnetic and magnetotransport properties of La0.8Sr0.2MnO3 composite. *J. Alloys Compd*, *437*, 22–26. https://doi.org/10.1016/j.jallcom.2006.07.104

Hon, X. T., Lau, L. N., Lim, K. P., Kechik, M. M. A., Chen, S. K., Shabdin, M. K., Miryala, M., & Shaari, A. H. (2024). The magnificent manifestation of Nd0.7Sr0.3MnO3 ceramics: A comprehensive exploration of different wet chemical routes via sol-gel and thermal treatment methods. *Journal of Alloys and Compounds*, *1004*, 175733. https://doi.org/10.1016/j.jallcom.2024.175733

Hwang, H., Cheong, S., Ong, N., & aB. (1996). Batlogg, Spin-polarized intergrain tunneling in La2/3Sr1/3MnO3, Phys. *Rev. Lett*, *77*. https://doi.org/10.1103/PhysRevLett.77.2041

Lau, L. N., Lim, K. P., Chok, S. Y., Ishak, A. N., Hon, X. T., Wong, Y. J., Kechik, M. M. A., Chen, S. K., Ibrahim, Nb., Miryala, M., Murakami, M., & Shaari, A. H. (2021). Effect of NiO Nanoparticle Addition on the Structural, Microstructural, Magnetic, Electrical, and Magneto-Transport Properties of La0.67Ca0.33MnO3 Nanocomposites. *Coatings*, *11*, 835. https://doi.org/10.3390/coatings11070835

Lau, L. N., Lim, K. P., Ishak, A. N., Kechik, M. M. A.,

Chen, S. K., Ibrahim, Nb., Miryala, M., Murakami, M., & Shaari, A. H. (2021). The Physical Properties of Submicron and Nano-Grained La0.7Sr0.3MnO3 and Nd0.7Sr0.3MnO3 Synthesised by Sol–Gel and Solid-State Reaction Methods. *Coatings*, *11*(3), 361. https://doi.org/10.3390/coatings11030361

Lau, L. N., Lim, K. P., Ngai, L. M., Ishak, A. N., Kechik, M. M. A., Chen, S. K., Ibrahim, N. B., & Shaari, A. H. (2020). Influence of Al2O3 on the low-field magnetoresistance of sol–gel grown La0.67Ca0.33MnO3: Al2O3 nanocomposites. *Applied Physics A*, *126*, 1–7. https://doi.org/10.1007/s00339-020-03924-5

Li, J., Chen, Q., Yang, S., Yan, K., Zhang, H., & Liu, X. (2019). Electrical transport properties and enhanced broad-temperature-range low field magnetoresistance in LCMO ceramics by Sm2O3 adding. *J. Alloys Compd*, *790*, 240–247. https://doi.org/10.1016/j.jallcom.2019.03.169

Modi, A., Bhat, M. A., Pandey, D. K., Tarachand, S. B., Gaur, N. K., & Okram, G. S. (2017). Structural, magnetotransport and thermal properties of Sm substituted La0.7−xSmxBa0.3MnO3 (0≤x≤0.2) manganites. *Journal of Magnetism and Magnetic Materials*, *424*, 459–466. https://doi.org/10.1016/j.jmmm.2016.10.048

Nagaev, E. L. (2001). Colossal-magnetoresistance materials: manganites and conventional ferromagnetic semiconductors. *Physics Reports*, *346*, 387–531. https://doi.org/10.1016/S0370-1573(00)00111-3

Navin, K., & Kurchania, R. (2018). Structural, magnetic and transport properties of the La0.7Sr0.3MnO3-ZnO nanocomposites. *Journal of Magnetism and Magnetic Materials*, *448*, 228–235. https://doi.org/10.1016/j.jmmm.2017.06.035

Ng, S., Lim, K., Halim, S., & Jumiah, H. (2018). Grain size effect on the electrical and magneto-transport properties of nanosized Pr0.67Sr0.33MnO3. *Results in Physics*, *9*, 1192–1200. https://doi.org/10.1016/j.rinp.2018.04.032

Phong, P. T., Khiem, N. V, Dai, N. V, Manh, D. H., Hong, L. V, & Phuc, N. X. (2009). Influence of Al2O3 on low-field spin-polarized tunneling magnetoresistance of (1−x) La0.7Ca0.3MnO3+x Al2O3 composites. *Mater. Lett*, *63*, 353–356. https://doi.org/10.1016/j.matlet.2008.10.035

Sadhu, A., & Bhattacharyya, S. (2014). Enhanced Low-Field Magnetoresistance in La0.71Sr0.29MnO3 Nanoparticles Synthesized by the Nonaqueous Sol–Gel Route. *Chemistry of Materials*, *26*, 1702–1710. https://doi.org/10.1021/cm4041665

Staruch, M., Gao, H., Gao, P.-X., & Jain, M. (2025). Low-Field Magnetoresistance in La0.67Sr0.33MnO3:ZnO Composite Film, Adv. *Advanced Functional Materials*, *22*, 3591–3595. https://doi.org/10.1002/adfm.201200489

Tang, T., Tien, C., & Hou, B. (2008). Low-field magnetoresistance of Ag-substituted perovskite-type manganites. *Physica B: Condensed Matter*, *403*, 2111–2115. https://doi.org/10.1016/j.physb.2007.11.020

Thanh, T. D., Phong, P. T., Dai, N. V, Manh, D. H., Khiem, N. V, Hong, L. V, & Phuc, N. X. (2011). Magneto-transport and magnetic properties of (1–x)La0.7Ca0.3MnO3+xAl2O3 composites. *Journal of Magnetism and Magnetic Materials*, *323*, 179–184. https://doi.org/10.1016/j.jmmm.2010.08.060

Xia, W., Pei, Z., Leng, K., & Zhu, X. (2020). Research Progress in Rare Earth-Doped Perovskite Manganite Oxide Nanostructures. *Nanoscale Research Letters*, *15*, 1–55. https://doi.org/10.1186/s11671-019-3243-0

Zener, C. (2018). Interaction between the d-shells in the transition metals. II. Ferromagnetic compounds of manganese with perovskite structure. *Physical Review*, *82*(3), 403. https://doi.org/10.1103/PhysRev.82.403

Zhou, Y., Zhu, X., & Li, S. (2017). Structure, magnetic, electrical transport and magnetoresistance properties of La0.67Sr0.33Mn1−xFexO3 (x=0–0.15) doped manganite coatings. *Ceramics International*, *43*, 3679–3687. https://doi.org/10.1016/j.ceramint.2016.11.210

Zi, Z., Fu, Y., Liu, Q., Dai, J., & Sun, Y. (2012). Enhanced low-field magnetoresistance in LSMO/SFO composite system. *Journal of Magnetism and Magnetic Materials*, *324*, 1117–1121. https://doi.org/10.1016/j.jmmm.2011.10.033